A closed-loop brain–machine interface framework design for motor rehabilitation

Hongguang Pan [a], Wenyu Mi [a], Xinyu Lei [a], Jun Deng [b],*

[a] *College of Electrical and Control Engineering, Xi'an University of Science and Technology, Xi'an 710054, China*
[b] *College of Safety Science and Engineering, Xi'an University of Science and Technology, Xi'an 710054, China*

ARTICLE INFO

ABSTRACT

Brain–machine interfaces (BMIs) can be adopted to rehabilitate motor systems for disabled subjects by sensing cortical neuronal activities and creating new method. In this paper, to achieve the function of motor rehabilitation, two generalized BMI frameworks, including decoders, encoders and auxiliary controllers, are proposed and compared based on a classical single-joint information transmission model. Firstly, a decoder based on the Wiener filter and an encoder based on a network of spiking neurons are designed to compensate for the absent information pathway, and a charge-balanced intra-cortical microstimulation current is chosen as the input of the spiking neuron network; Secondly, to formulate closed-loop BMI frameworks, two auxiliary controllers are designed according to the strategy of model predictive control, where the controller inputs are the position of joint muscle trajectories and the average firing activity trajectories of perceived position vector neurons. Thirdly, considering that several integer parameters are included in the charge-balanced intra-cortical microstimulation current and that the optimization problem for solving the control inputs also includes these decision variables, a particle swarm optimization algorithm is adopted to solve the hard optimization problem. We compare the motor recovery effectiveness of the two presented frameworks through these simulations and choose the better framework for future BMI system design. The proposed frameworks provide a important theoretical guidance for designing BMI system applied in future life.

1. Introduction

As an interactive system, a brain–machine interface (BMI) can create a new way and transmit the information from the brain to external independent of the spinal cord and muscles [1–3]. In BMIs, the cortical neuron activity is recorded and used to assist in the daily life of disabled patients, restore their impaired motor tasks and so on [2–6]. A typical BMI system (see Fig. 1) mainly consists of the following components: the brain, a decoder, an encoder and an external device (e.g., artificial arm) [1,7,8]. The decoder is used to record the activities of cortical neurons and convert them for use by an external device, and the encoder is used to convert the external state of the device to information that can be received by the brain.

Many studies on BMI-based devices with healthy subjects have been extensively performed in the last two decades [2,3,5,9–11]. Among these studies, in open-loop BMI systems, which do not use an encoder, the external device cannot track the desired trajectory accurately [2,10,11]. The main reason for this is the lack of an encoder, i.e., an information feedback pathway between the brain and the external device [2,5,10,12]. Dangi and Sussillo tested the position recovery effect of a BMI system with an adaptive Kalman filter-based decoder and with a recursive neural network-based decoder in the presence of a feedback pathway, respectively. The results showed that adding the feedback pathway can improve the position recovery accuracy [13,14]. These results are also consistent with those found in [2,10,15–17]. Furthermore, Orsborn et al. noted that an auxiliary controller should be introduced to improve the position recovery effect of a BMI system because electroencephalograms (EEGs) change during the time of joint movement [16]. This is consistent with observations made in [2]. Hence, to develop the next generation of BMIs, a systematic framework including an encoder (feedback pathway) and an auxiliary controller is highly imperative [2,18].

Encoders are typically designed to produce output as the average firing rate, a standard feature of neurons that has been used to described the performance of cortical neurons for nearly 90 years [19]. Using a spiking neuron network with many neurons to obtain

Fig. 1. The closed-loop BMI system.

Fig. 2. The SJIT model (diagram redrawn from Fig. 1.1 in [31]).

Table 1
The abbreviations and full names in the SJIT model.

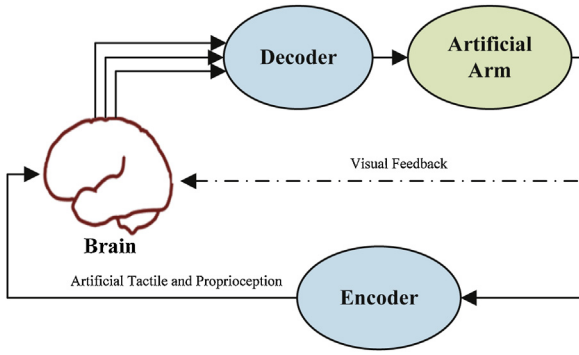| Abbreviation	Full name
DVV	Desired velocity vector
OPV	Outflow position vector
OFPV	Outflow force and position vector
SFV	Static force vector
IFV	Inertial force vector
PPV	Perceived position vector
DV	Difference vector
TPV	Target position vector

information about brain activity is more meaningful and effective than using a single neuron [19,20]. When current stimulates the neuron network, each neuron receives the same current and starts firing, and the network can provide the average firing rate to the brain and feedback the external information. In this paper, a spiking neuron network is adopted to design the encoder and acquire the average firing rate. Furthermore, intra-cortical micro-stimulation (ICMS) (as the encoder input) has been regarded as a potential technology to offer artificial sensation to the brain [10,21–23]. This technology has been widely used in many fields, such as vestibular prosthesis [17], cochlear implants [24], retinal prosthesis [25] and BMIs [1,26]. In this paper, this technology is used to generate the stimulating current.

In this paper, model predictive control (MPC) is chosen to design the auxiliary controller because of the following advantages [27–29]: (1) its performance indicators can be flexibly selected to compensate for the cost function and to optimize performance by receding horizon optimization; (2) both the system model and constraints can be taken into account and processed in an optimization problem; (3) the stability, robustness and other qualities achieved in MPC can be conveniently extended to the analysis of closed-loop BMI systems. Then, we can formulate the closed-loop framework using the above chosen auxiliary controller. The formulation of closed framework is very important, because (1) it can provide necessary guidance for the subsequent design of a BMI system and is conducive to solving the problem of poor compatibility among various parts of the BMI; (2) it can allow the theoretical analysis of the stability, robustness and uncertainty caused by data transmission delays or model mismatches. Hence, based on the decoder, spiking neuron network encoder, MPC auxiliary controller, two closed-loop frameworks are formulated in this paper.

The main contributions of this paper are as follows. First, an encoder based on ICMS technology and a spiking neuron network is designed to deliver the states of the external devices to the brain; a Wiener filter-based decoder designed in our previous work is introduced to compensate for the information pathway from the brain to the external device [30]. Second, two closed-loop frameworks are formulated based on the decoder, the encoder, and auxiliary controllers. Note that the difference between these two frameworks is the inputs of auxiliary controllers: one is the position trajectories of joint muscles, and the other is the average firing activity trajectories of perceived position vector neurons. Third, the ICMS current contains several integer parameters that are also decision variables for the designed optimization problems, which make the optimization problems difficult to solve, hence, a heuristic population-based search algorithm, particle swarm optimization (PSO), is used to solve the optimization problems from the two frameworks. In addition, the motor rehabilitation effectiveness comparison of these two frameworks is given, and the second designed BMI framework can recover the motor function of the joint much better than
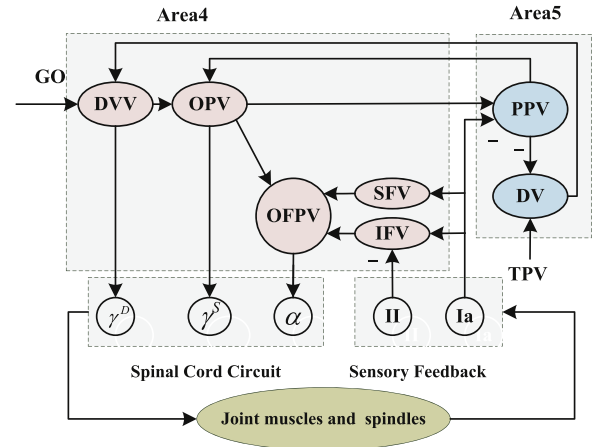
that of the first framework. The proposed frameworks provide an important theoretical guidance for designing BMI system applied in future life.

2. SJIT model

Bullock et al. proposed a single-joint information transmission (SJIT) model shown in Fig. 2 [31]. This model shows the essential cortical pathways for voluntary single-joint movement.

Here, we briefly introduce the SJIT model; the related abbreviations and their full names are shown in Table 1. In the whole process of joint motion, the "DV" neurons calculate the difference vector between the perceived joint position from the "PPV" neurons and the target joint position from the nerve centre continuously. The activity of the "DV" neurons can be described by:

$$r_i(t) = \max\{T_i - x_i(t) + B^r, 0\}, \tag{1}$$

where t is continuous time, $0 \le r_i(t) \le 1$ is the average firing activity of the neurons related to agonist muscle i, B^r represents the baseline firing activity of these neurons, $x_i(t)$ is the average firing activity of the "PPV" neurons, and T_i is the average firing activity of the "TPV" neurons. Note that the subscript i in this paper indicates the activity related to agonist muscle i, and the subscript j indicates the activity related to antagonist muscle throughout this paper.

The computed difference vector is transmitted to the "DVV" neurons. The activity of the "DVV" neurons can be described by

$$u_i(t) = \max\{g(t).(r_i(t) - r_j(t) + B^u, 0\}, \tag{2}$$

where $u_i(t)$ is the average firing rate of these neurons, B^u shows the baseline firing activity of these neurons, and $g(t)$ represents the "GO" signal in Fig. 2. GO signal is generated from the basal ganglia, can control the magnitude of the "DVV" vector without altering its direction, and thus can be used to scale the velocity of movement

[31]. The "GO" signal does not change suddenly, and a two-step cellular cascade is used to show the dynamics of it,

$$\frac{dg^1(t)}{dt} = \epsilon(-g^1(t) + (C - g^1(t))g^0), \tag{3a}$$

$$\frac{dg^2(t)}{dt} = \epsilon(-g^2(t) + (C - g^2(t))g^1(t)), \tag{3b}$$

$$g(t) = g^0 \frac{g^2(t)}{C}, \tag{3c}$$

where ϵ is a constant that represents slow integration, C is the saturation value, and g^0 is a constant from a forebrain decision center, which can determine the magnitude of the "GO" signal.

"OPV" is related to the tonic neurons and shows the outflow position. The activity of the "OPV" neurons can be described by

$$\frac{dy_i(t)}{dt} = (1 - y_i(t))(\eta x_i(t) + \max\{u_i(t) - u_j(t), 0\})$$
$$- y_i(t)(\eta x_j(t) + \max\{u_j(t) - u_i(t), 0\}), \tag{4}$$

where $y_i(t)$ is the average firing rate of the "OPV" neurons and η is a scaling factor.

Static ($\gamma_i^S(t)$) and dynamic ($\gamma_i^D(t)$) gamma motoneurons are used to convey the commands from the brain to the joint. The activity of these motoneurons can be described by

$$\gamma_i^S(t) = y_i(t), \tag{5a}$$

$$\gamma_i^D(t) = \rho \max\{u_i(t) - u_j(t), 0\}, \tag{5b}$$

where ρ is a scaling parameter.

The primary ("Ia") and secondary ("II") muscle spindle afferents are used to convey joint position information to the "PPV" neurons, which can be modeled as:

$$s_i^1(t) = S(\theta \max\{\gamma_i^S(t) - p_i(t), 0\} + \phi \max\{\gamma_i^D(t)$$
$$- \frac{dp_i(t)}{dt}, 0\}), \tag{6a}$$

$$s_i^2(t) = S(\theta \max\{\gamma_i^S(t) - p_i(t), 0\}), \tag{6b}$$

where $s_i^1(t)$ is the average firing activity of the primary spindle afferents, $s_i^2(t)$ is the average firing activity of the secondary spindle afferents, $p_i(t)$ is the agonist muscle position, θ represents the sensitivity of the nuclear chain fibres and the static nuclear bag fibres, ϕ represents the sensitivity of the dynamic nuclear bag fibres, and $S(\omega) = \omega/(1 + 100\omega^2)$.

The activity of the "PPV" neurons can be described by

$$\frac{dx_i(t)}{dt} = (1 - x_i(t)) \max\{\Theta y_i(t) + s_j^1(t - \tau) - s_i^1(t - \tau),$$
$$0\} - x_i(t) \max\{\Theta y_j(t) + s_i^1(t - \tau) - s_j^1(t - \tau), 0\}, \tag{7}$$

where Θ represents the constant gain and τ represents the delay time of spindle feedback.

The activity of the "IFV" neurons and the "SFV" neurons can be described by

$$q_i(t) = \lambda_i \max\{s_i^1(t - \tau) - s_i^2(t - \tau) - \Lambda, 0\}, \tag{8}$$

$$\frac{df_i(t)}{dt} = (1 - f_i(t))hs_i^1(t - \tau) - \psi f_i(t)(f_j(t) + s_j^1(t - \tau)), \tag{9}$$

where $q_i(t)$ is the average firing rate of the "IFV" neurons and $f_i(t)$ is the average firing rate of the "SFV" neurons, Λ represents a constant threshold, h controls the speed and strength of an external load compensation, and ψ is a parameter scaling by the antagonist component. The "OFPV" neurons provide a phasic-tonic activity and can be described by
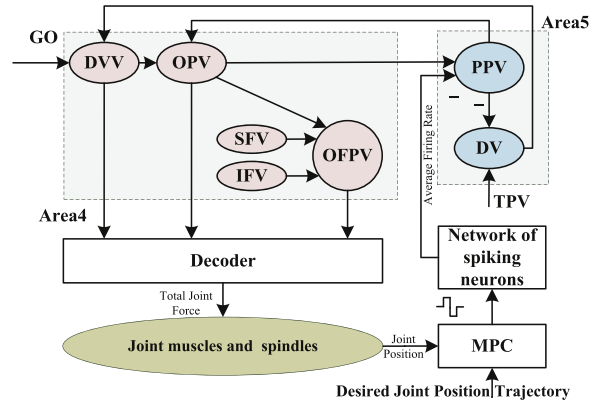
$$a_i(t) = y_i(t) + q_i(t) + f_i(t), \tag{10}$$

Fig. 3. Designed framework 1.

where $a_i(t)$ is the average firing activity of the "OFPV" neurons. The alpha motoneurons can be modeled as

$$\alpha_i(t) = a_i(t) + \delta s_i^1(t), \tag{11}$$

where $\alpha_i(t)$ is the average firing rate of the alpha motoneurons and δ represents the stretch reflex gain.

The joint dynamics can be described by

$$\frac{d^2 p_i(t)}{dt^2} = \frac{1}{I}\left(\Delta M(t) + E_i - V \frac{dp_i(t)}{dt}\right), \tag{12}$$

where $\Delta M(t) = \max\{c_i(t) - p_i(t), 0\} - \max\{c_j(t) - p_j(t), 0\}$ is the generated total force of the muscles, $p_i(t) + p_j(t) = 1$, I represents the joint inertia moment, V represents the viscosity of the joint, and E_i represents the external force imposed on the joint. $c_i(t)$ represents the activity of muscle contraction and can be described by

$$\frac{dc_i(t)}{dt} = \nu(-c_i(t) + \alpha_i(t)), \tag{13}$$

where ν is the contraction rate of the muscles.
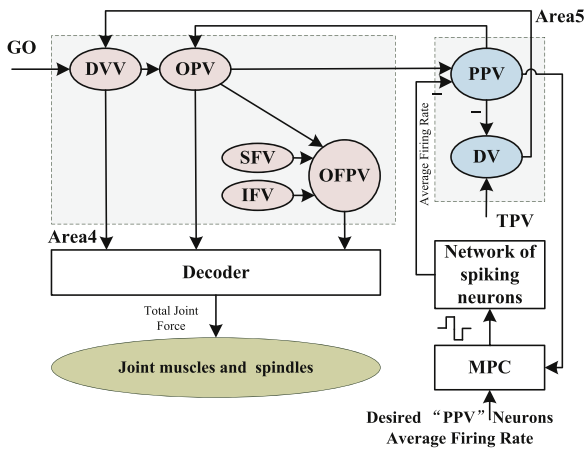
3. Two closed-loop BMI frameworks

As shown in Fig. 2, the command from the brain can be delivered to the joint through the spinal cord circuit; the "PPV" neurons receive proprioceptive feedback (II, Ia) information and perceive the present position of the joint. In a BMI framework, these two information pathways should be compensated. In our previous work, a decoder based on the Wiener filter was designed to compensate for the absence of a spinal cord circuit (see [30]). In this work, a spiking neuron network and ICMS-current technology are used to compensate for the absent proprioceptive feedback information. Then, two closed-loop BMI frameworks are formulated based on the decoder, a spiking neuron network (encoder), ICMS-current technology, and an auxiliary controller (see Figs. 3 and 4).

3.1. Decoder design

The Wiener filter-based decoder is briefly reviewed here. This decoder is trained by a data driven method, and the sampling time T_s is chosen as 30 ms to obtain the training data set. See Section 3 in [30] for details.

It can be assumed that the relationship between the total force and firing rate of cerebral cortex neurons is as follows:

$$\Delta M(k) = \sum_{l=0}^{L-1} \sum_{m=1}^{N} z_m(k - l)w_{ml} \tag{14}$$

Fig. 4. Designed framework 2.

where $k = 1, 2, \ldots$ is discrete time, $\Delta M(k)$ and $z(k)$ are the recorded ΔM and the average firing rate of neurons at time k, respectively, L is the discrete delay time, m is the index of the neuron population, N is the number of recorded neuron populations, and w_{ml} is the weight. The vector form of (14) is

$$\Delta M(k) = \mathbf{w}^{\mathrm{T}} \mathbf{z}(k) \tag{15}$$

where $\mathbf{w}$ is the weight matrix with dimensions $L \times N \times 1$, and $\mathbf{z}(k) = [z_1(k), z_1(k-1), z_1(k-L+1), z_2(k), z_2(k_1), z_2(k-L+1), \ldots, z_N(k-L+1)]$. We set $N = 6, L = 10, z_1 = y_i, z_2 = y_j, z_3 = u_i, z_4 = u_j, z_5 = a_i,$ and $z_6 = a_j$ in this work.

3.2. Charge-balanced biphasic ICMS current

In the charge-balanced biphasic ICMS current, the injected positive charge is equal to the negative charge. To reduce the damage of external stimulation to the brain, charge-balanced biphasic ICMS current is used to transfer information to the brain in this paper. The current is shown in the left plot of Fig. 5, where $a_1w_2 + a_2w_3 = 0$. The relevant parameters of the current can be obtained by the auxiliary controller when the closed loop is formulated later. The sampling time of the auxiliary controller is T_s ms. To reduce the complexity of the optimization problem (20), only one biphasic ICMS current is considered over one sampling period in this paper, i.e., $T_b = \sum_{l_n=1}^{4} w_{l_n} = T_s$ ms.

3.3. Network of spiking neurons (encoder) design

Because the "PPV" neurons cannot receive the ICMS current directly, to convert the biphasic ICMS current into the average firing rate that can be received by the "PPV" neurons, an encoder based on a spiking neuron network is used in this paper (see Fig. 5). Each

neuron in the network receives two types of currents, i.e., the ICMS current and the synaptic current $I_{i_n}^s(t)$. An integrate-and-fire (IF) model is used to represent each neuron in the network [19]. In the IF model,

$$\tau_m \frac{\mathrm{d}v_{i_n}(t)}{\mathrm{d}t} = -v_{i_n}(t) + RI_{i_n}(t), \tag{16}$$

where the subscript i_n indicates the i_nth neuron, $v_{i_n}(t)$ denotes the membrane potential, τ_m is a time constant, $I_{i_n}(t)$ is the received current, and R is the membrane resistance. v_{i_n} is reset to v^r whenever v_{i_n} exceeds the constant firing threshold vth, and the firing rate of the neuron is the number of times that v_{i_n} exceeds vth over a unit of time. The output of the network is the average firing rate r_c of all neurons in the network.

The total synaptic current $I_{i_n}^s(t)$ to the i_nth neuron can be modeled as:

$$I_{i_n}^s(t) = -g_{i_n}(t)(v_{i_n}(t) - \varsigma), \tag{17}$$

where ς is the excitatory membrane reversal potential and $g_{i_n}(t) \geq 0$ is the synaptic conductance, which can be modeled as:

$$g_{i_n}(t) = \sum_{j_n \neq i_n = 1}^{N_{neu}} \sum_{f_n} w_{j_n} F(t - t_{j_n}^{f_n}), \tag{18}$$

where N_{neu} represents the number of presynaptic neurons, w_{j_n} is synaptic weight between the j_nth presynaptic neuron and the i_nth post-synaptic neuron, $t_{j_n}^{f_n}$ is the time at which the f_nth incoming action potential arrives from the j_nth presynaptic neuron to the i_nth post-synaptic neuron, F is a function of $t - t_{j_n}^{f_n}$, which represents the stereotypical time course of postsynaptic conductances following presynaptic spikes and can be described by
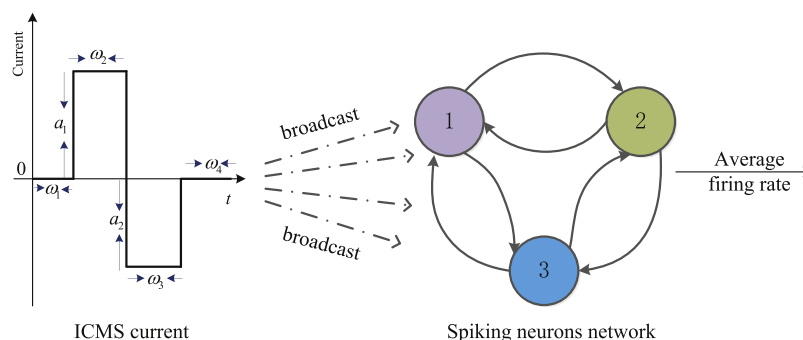
$$F(t - t_{j_n}^{f_n}) = \frac{q_{j_n}}{\tau_{j_n}}(t - t_{j_n}^{f_n}) \exp\left(-\frac{t - t_{j_n}^{f_n}}{\tau_{j_n}}\right) \Theta(t - t_{j_n}^{f_n}), \tag{19}$$

where q_{j_n} is the maximum conductance from the j_nth neuron, τ_{j_n} is the synaptic time constant, and $\Theta(t - t_{j_n}^{f_n})$ is the Heaviside step function.

3.4. Auxiliary controller design

In the two closed-loop frameworks shown in Figs. 3 and 4, the auxiliary model predictive controllers are used to design the artificial feedback pathways by determining the parameters of the biphasic ICMS current. Note that, in framework 1, the inputs of the auxiliary controller are the position of the joint muscle, and in framework 2, the inputs of the auxiliary controller are the average firing activity trajectories of the perceived position vector neurons.

For the auxiliary controller based on the MPC strategy, suitable predicted future outputs $O(k + m + 1 \mid k)$ ($m = 0, 1, 2, \ldots, N_p - 1$)

Fig. 5. The process of encoding the ICMS current.

and the corresponding N_c control inputs can be found by minimizing the cost function $\mathbb{J}_p(k)$ at each sampling time k; here, N_c and N_p are the control horizon and predictive horizon, respectively. However, only the first control input can be applied in the actual system at this sampling time. At sampling time $k+1$, the optimization problem is solved again according to the new state [32].

For framework 1 (Fig. 3), the optimization problem of the auxiliary model predictive controller is formulated as follows:

$$\min_{a_1(k+l_t|k), a_2(k+l_t|k), w_{l_n}(k+l_t|k)} \mathbb{J}_p(k) \tag{20a}$$

$$\text{s.t.} (1) - (10), (12), (14), (16) - -(19), \tag{20b}$$

$$T_s = \sum_{l_n=1}^{4} w_{l_n}(k+l_t|k), \tag{20c}$$

$$a_1(k+l_t|k)w_2(k+l_t|k) + a_2(k+l_t|k)w_3(k+l_t|k) = 0, \tag{20d}$$

$$a_1(k+l_t|k) \in [0\,\overline{a}], \tag{20e}$$

$$a_2(k+l_t|k) \in [\underline{a}\,0], \tag{20f}$$

where $l_t \in \{0, 1, \ldots, N_c - 1\}$, $l_n \in \{1, 2, 3, 4\}$, $\overline{a} = -\underline{a} = 10,000$, $\mathbb{J}_p(k) = \sum_{m=0}^{N_p-1}(O(k+m+1\mid k) - R(k+m+1\mid k))^2$ is the cost function, $O(\cdot)$ is the predicted future position of agonist muscle i, i.e., $p_i(\cdot)$, and $R(\cdot)$ represents the desired position trajectory.

Note that in optimization problem (20), the continuous time t in (1)–(10), (12), and (16)–(19) can be transformed into discrete time k through a sampling operation with sampling time T_s; more details can be found in our previous work [30].

For framework 2 (Fig. 4), the form of the formulated optimization problem and the meaning of parameters N_c, N_p, T_s, l_t, l_n, $\overline{a}$, $-\underline{a}$ are the same as in (20). However, in $\mathbb{J}_p(k)$, $O(\cdot)$ is the really average firing activity of the "PPV" neurons, and $R(\cdot)$ is the desired average firing activity of the "PPV" neurons. The desired position trajectory and firing activity trajectory are obtained by the SJIT model (i.e., (1)–(13)).

When the decision variables are solved, the biphasic ICMS current can be generated. The current is then delivered to the spiking neuron network, converted into the average firing rate r_c, and then applied to the "PPV" neurons, i.e., (7) is replaced by (21),

$$\frac{dx_i(t)}{dt} = (1 - x_i(t))\max\{\Theta y_i(t) - r_c, 0\}$$
$$-x_i(t)\max\{\Theta y_j(t) + r_c, 0\}. \tag{21}$$

4. Solving the optimization problems

Both optimization problems in the designed frameworks have integer decision variables. Hence, for the purpose of solving these two optimization problems, the PSO algorithm is adopted in this work.

A brief introduction of the PSO is given as follows [33]. An individual particle S' ($S' \in \{1, 2, \ldots, S'_n\}$) consists of three parts: a position vector ($X_{S'} = \{X_{S'1}, X_{S'2}, \ldots, X_{S'D_n}\}$), a best position vector that is determined individually ($P_{S'} = \{P_{S'1}, P_{S'2}, \ldots, P_{S'D_n}\}$), and a velocity vector ($V_{S'} = \{V_{S'1}, V_{S'2}, \ldots, V_{S'D_n}\}$). Here, D_n indicates the number of dimensions. The update rules for the particle position and velocity in each dimension are as follows:

$$V_{S'D}(k'+1) = \omega(k')V_{S'D}(k') + C_p\varepsilon_1(k')(P_{S'D}(k')$$
$$-X_{S'D}(k')) + C_p\varepsilon_2(k')(P_{gD}(k') - X_{S'D}(k')), \tag{22}$$

$$X_{S'D}(k'+1) = X_{S'D}(k') + V_{S'D}(k'+1), \tag{23}$$

where k' is the iteration; ε_1 and ε_2 are two unique parameters randomly generated in $(0, 1)$ in each update; C_p is a positive constant (set to 2 in this paper); $D \in \{1, \ldots, D_n\}$; and $P_g(k') =$

$\{P_{g1}(k'), P_{g2}(k'), \ldots, P_{gD_n}(k')\}$ is a vector which indicates the global best position at k'.

In this work, the biphasic current can be determined by 6 parameters, i.e., a_1, a_2 and w_1, w_2, w_3, w_4. However, considering $\sum_{l_n=1}^{4} w_{l_n} = T_s$ and $a_1 w_2 + a_2 w_3 = 0$, the biphasic current only has 4 degrees of freedom. Here, we chose a_1, w_1, w_2, w_3 as the operating variables, i.e., the optimization problem (20) includes $4 \times N_c$ independent decision variables. When the PSO algorithm is adopted to solve the designed optimization problems, the particle position $X_{S'D}$ is a vector composed of a_1, w_1, w_2, w_3. The particle fitness function is equal to $\mathbb{J}_p(k)$ at each k. The update rule for $\omega(k')$ is

$$\omega(k') = 0.2 + k'\frac{1.8 - 0.2}{K'_{max}}, \tag{24}$$

where K'_{max} is the maximum number of iterations.

It should be noted that in the process of updating the particles, the constraints in the optimization problem (20) may be seriously violated. To solve this problem, w_1, w_2, w_3, w_4 are set as positive integer variables, and an algorithm is designed in this paper to ensure that the particles satisfy the constraints in optimization problem (20).

Algorithm 1. (Constraint-update algorithm)

(1) if $k' = 1$, for each particle S' satisfying (20e) and (20f), generate particle position $X_{S'} = (a_1, w_1, w_2, w_3)$ randomly; if $k' > 1$, update the position of the particle (a_1, w_1, w_2, w_3);
(2) confirm a_1: if a_1 satisfies (20e), hold it; else, let a_1 be equal to the nearer bound;
(3) confirm w_2: according to (20c) and (20f), $w_3 \geq \frac{a_1 w_2}{10,000}$, $w_3 \leq 30 - w_2$ and $w_2 \geq 0$; then, $w_2 \in \left[0\,\frac{30 \times 10,000}{10,000+a_1}\right]$ can be obtained. Because w_2 is an integer, the constraint above should be changed to $w_2 \in \left[0\,\text{int}\left(\frac{30 \times 10,000}{10,000+a_1}\right)\right]$ (where int($\cdot$) means nearest integer). If w_2 satisfies this constraint, let $w_2 = \text{int}(w_2)$; else, let w_2 be equal to the nearer bound;
(4) confirm w_3: similar to the last step, $w_3 \in [\text{int}\left(\frac{a_1 w_2}{10,000}\right) 30 - w_2]$. If w_3 satisfies this constraint, let $w_3 = \text{int}(w_3)$; else, let w_3 be equal to the nearer bound;
(5) confirm w_1: according to (20c), $w_1 \in [0\,30 - w_2 - w_3]$, if w_1 satisfies this constraint, hold it; else, let w_1 be equal to the nearer bound.

To clearly explain the working process of the two designed BMI frameworks, the overall algorithm of these frameworks is given as follows.

Algorithm 2. (Overall algorithm) Off-line stage,

(1) choose the parameters in the BMI frameworks and then acquire the desired trajectories $R(\cdot)$ by (1)–(13);
(2) provide the values of $\overline{a}$, $\underline{a}$ and T_s in the biphasic waveform of the charge-balanced ICMS current;
(3) provide the iteration step K'_{max} and particle number S'_n;
(4) choose the simulation step K_{max};

(1) provide an initial particle position $X_{S'}$ ($S' = 1, 2, \ldots, S'_n$) satisfying (20c)–(20f);
(2) if $k' = 1$, choose the prediction and control horizons N_p and N_c, calculate $O(k\mid k)$, $O(k+1\mid k)$, $\ldots$, $O(k+N_p-1\mid k)$ and $\mathbb{J}_p(k)$ for each $X_{S'}$, update $P_{S'}(k')$ and $P_g(k')$, and skip to 5;
(3) update $X_{S'}(k')$ and $\omega(k')$ through (22)–(24);
(4) choose the prediction and control horizons N_p and N_c, calculate $O(k\mid k)$, $O(k+1\mid k)$, $\ldots$, $O(k+N_p-1\mid k)$ and $\mathbb{J}_p(k)$ for each X'_S, and update $P'_S(k')$ and $P_g(k')$;
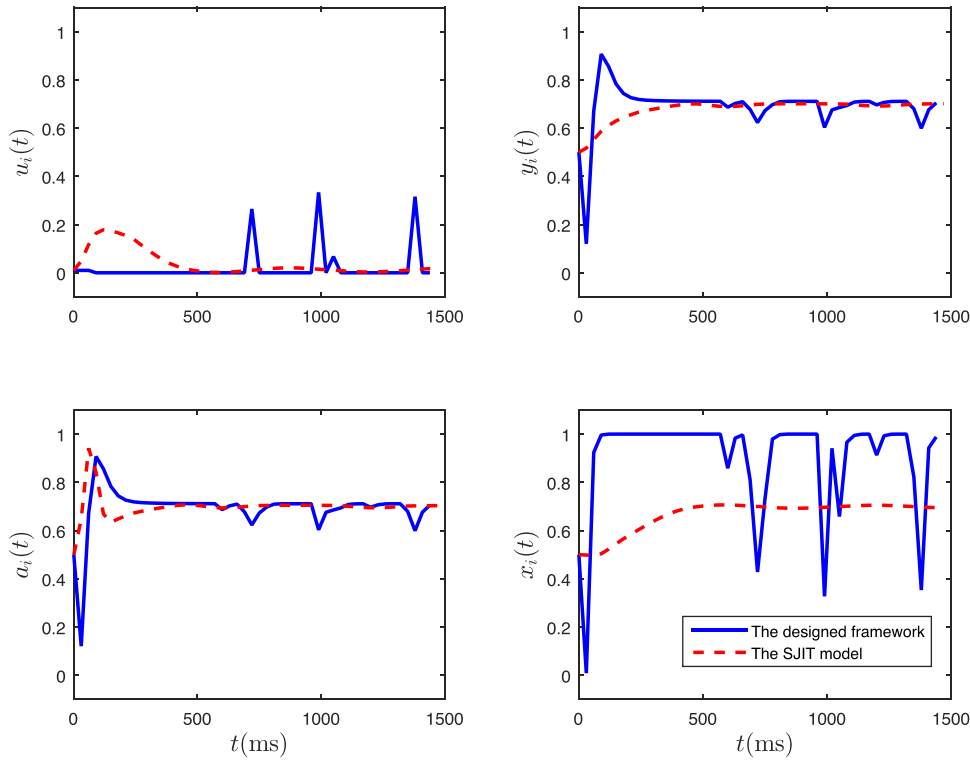
Fig. 6. The trajectories of u_i, y_i, a_i, x_i in framework 1.

(5) if $k' = K'_{max}$, the control input (i.e., the charge-balanced biphasic ICMS current $\{a_1, a_2, w_1, w_2, w_3, w_4\}$) is equal to $P_g(k')$; if not, $k' = k' + 1$ and return to 2);

(6) if $k > K_{max}$, impose the control input (i.e., $\{a_1, a_2, w_1, w_2, w_3, w_4\}$), calculate the system output, and stop; if not, $k = k + 1$ and return to (1);

Remark 1. During the tracking process, the position trajectory of the joint includes a rising stage and a stable stage. These two stages can be observed in the desired position trajectory $R(\cdot)$. In the first 480 ms, the joint position is as the rising stage; after 480 ms, the joint position is as the stable stage. The controller parameters N_p and N_c are chosen online.

5. Simulation results and further discussion

In this section, a series of simulations are designed to test and compare the two proposed frameworks. The sampling time T_s was chosen as 30 ms. The initial values of variables are set as follows: $y_i(0) = y_j(0) = 0.5$, $x_i(0) = x_j(0) = 0.5$, $p_i(0) = p_j(0) = 0.5$, $u_i(0) = u_j(0) = B^u$, $r_i(0) = r_j(0) = B^r$. Except for these, the initial values of other variables are all set to 0. The parameters in these two frameworks are set as follows: $I = 200$, $V = 10$, $v = 0.15$, $B^r = 0.1$, $B^u = 0.01$, $\Theta = 0.5$, $\theta = 0.5$, $\phi = 1$, $\eta = 0.7$, $\rho = 0.04$, $\lambda_1 = 150$, $\lambda_2 = 10$, $\Lambda = 0.001$, $\delta = 0.1$, $C = 25$, $\epsilon = 0.05$, $\psi = 4$, $h = 0.01$, $\tau = 0$ [31]. $S_n = 96$, $K'_{max} = 30$, $K_{max} = 49$. As mentioned in Remark 1, the position trajectory of the joint has a rising stage and a stable stage; for the rising stage, $N_p = 6$, $N_c = 3$, and for the stable stage, $N_p = 30$, $N_c = 15$. In the spiking neuron network, we set $N_{neu} = 3$, $\tau_m = 10$ ms, $R = 0.04$, $v_r = 65$ mV, $v_{th} = 45$ mV, $\varsigma = 0$. q_{j_n} ($j_n = 1, 2, 3$) for the agonist population and the antagonist population are set to $\{16.9610, 17.7975, 16.2787\}$, and $\{17.8244, 13.7881, 17.8530\}$, respectively. Similarly, the τ_{j_n} ($j_n = 1, 2, 3$) for these two populations are set to $\{5.1071, 7.5474, 7.8020\}$ and $\{5.8355, 6.6406, 7.8725\}$, respec-

tively. The weight matrices between the neurons are the same as those in [34]. Specifically, for the agonist population, the weight matrix is chosen as $\begin{pmatrix} 0 & 0.9572 & 0.1419 \\ 0.1576 & 0 & 0.4218 \\ 0.9706 & 0.8003 & 0 \end{pmatrix}$. For the antagonist population, the weight matrix is chosen as $\begin{pmatrix} 0 & 0.1419 & 0.7922 \\ 0.4854 & 0 & 0.9595 \\ 0.8083 & 0.9157 & 0 \end{pmatrix}$.

5.1. Simulation results

Figs. 6–9 shows the simulation results. As shown in Fig. 6, in framework 1, the average firing activities of the cerebral cortex neurons during the control process are significantly different from the natural activities acquired by the SJIT model. In Fig. 7, it can be seen that position output $p_i(t)$ of framework 1 cannot track the trajectory acquired from the SJIT model well; similarly, the velocity output cannot be tracked well either. Hence, framework 1 is not sufficient to recover the motor function of the artificial arm.

As shown in Fig. 8, in framework 2, the position tracking performance and average firing activities of the cerebral cortex neurons are much better than those in framework 1, although there are still some errors between the actual firing activity and the firing activity acquired by the SJIT model. In Fig. 9, it can be seen that framework 2 can track the position trajectory acquired from the SJIT model well; similarly, the velocity output can be recovered much better than by framework 1.

To compare the two frameworks, the sum of squares errors (SSEs) between the position trajectory of the SJIT model and the position output of the frameworks are used as evaluation criteria. The SSEs are shown in Table 2, and we can see that the conclusion from Table 2 is the same as that from Fig. 9, i.e., BMI framework 2 can recover the motor function of the joint much better than framework 1.
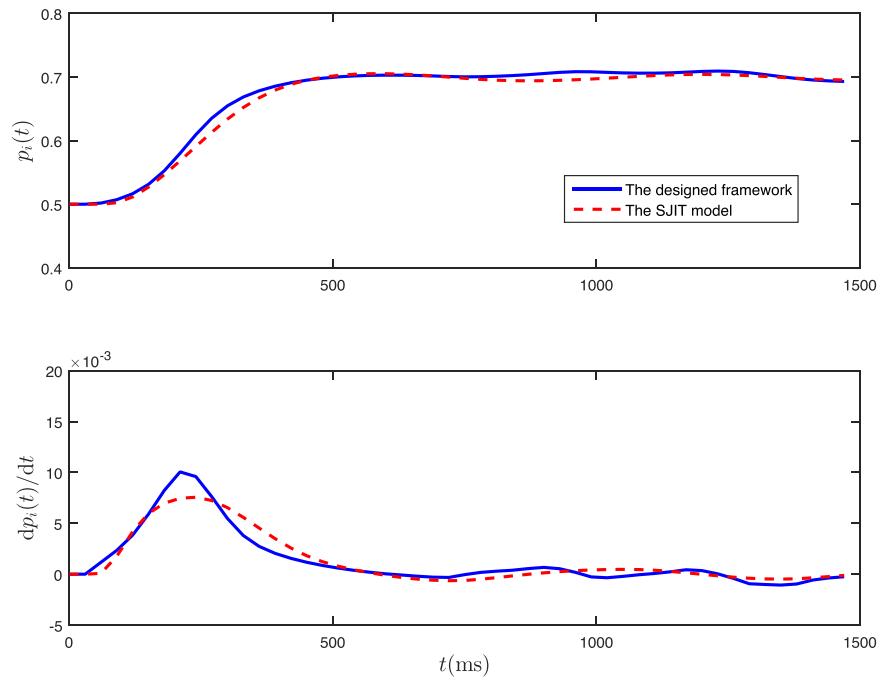
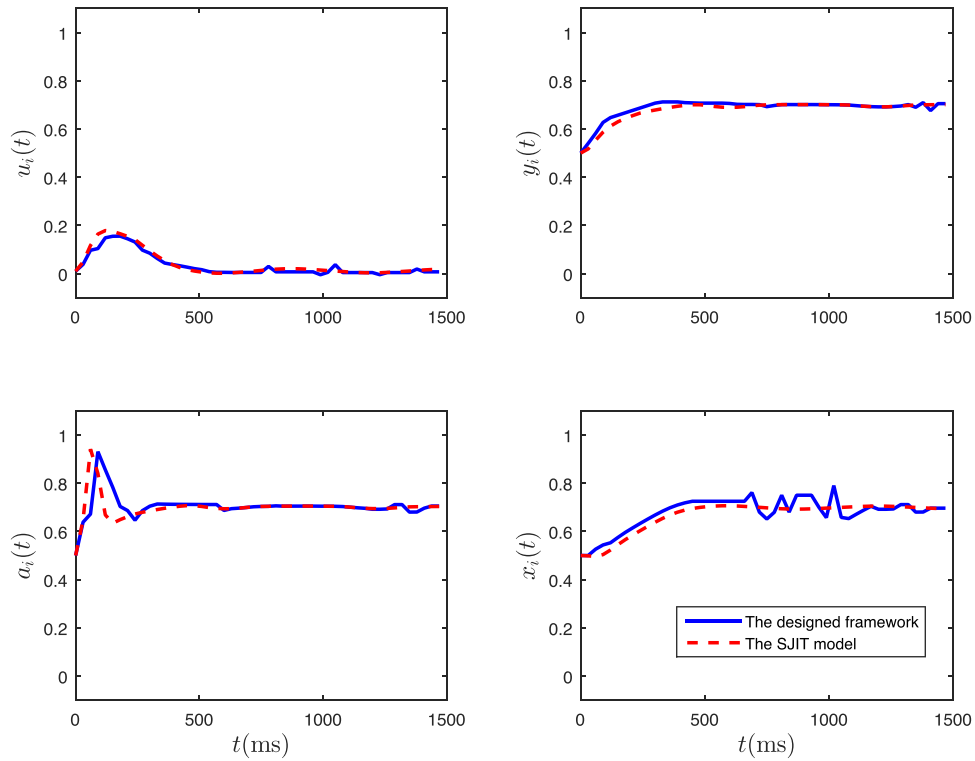**Fig. 7.** The trajectories of p_i, $\frac{dp_i(t)}{dt}$ in framework 1.

Fig. 8. The trajectories of u_i, y_i, a_i, x_i in framework 2.

Table 2
The SSEs of framework 1 and framework 2.

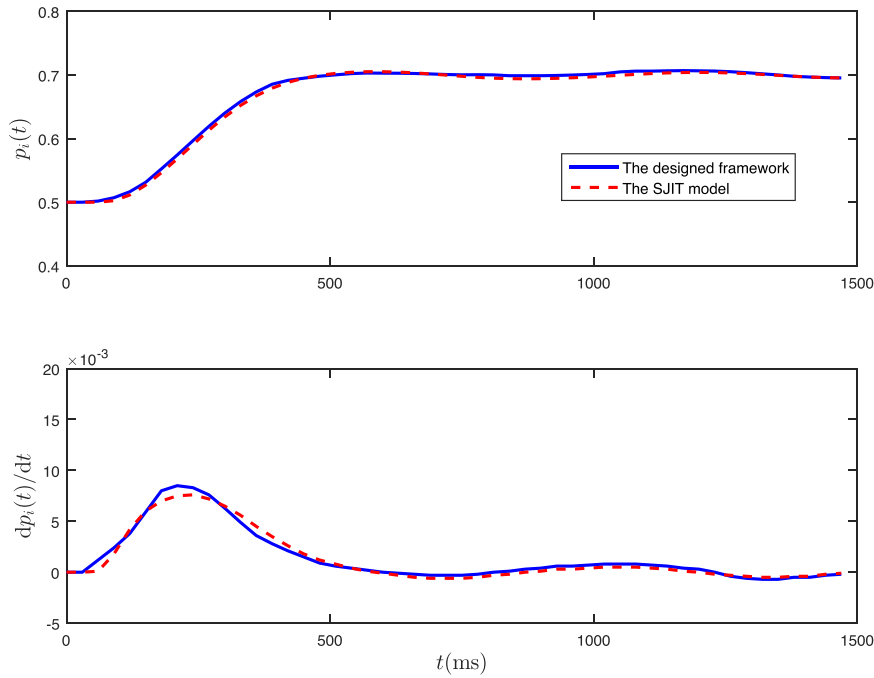|	u_i	y_i	a_i	x_i	p_i	dp_i
Framework 1	0.4723	0.4129	0.4654	4.8877	0.0031	3.1043×10^{-5}
Framework 2	0.0095	0.0117	0.1457	0.0525	0.0007	8.6700×10^{-6}

Fig. 9. The trajectories of p_i, $\frac{dp_i(t)}{dt}$ in framework 2.

5.2. Further discussion

Two frameworks based on the decoder, encoder, MPC-based auxiliary controllers are designed and compared in this paper. These two frameworks reconstruct the communication pathways between the brain and external device, and add auxiliary controllers, hence, they can give the guidance of the design of BMI system in the future. The reason for better performance of framework 2 and the discussion on the framework flexibility are analyzed in (1) and (2) as follows. There are also some limitations in the two designed frameworks, such as the existing of optimization problem bring lots of online computation burden, and the preliminary improvement in future work is show in (3).

(1) Reason for better performance. The only difference between the two designed frameworks is the inputs of the auxiliary controllers. The inputs to framework 2 are the average firing activity of the PPV neurons, and its tracking performance is much better than that of framework 1. The reason for this is that the average firing rate of the "PPV" neurons is correlated with the average firing activities a_i, a_j, u_i, u_j, y_i, and y_j directly. The accurate tracking of the average firing rate of the "PPV" neurons can improve the recovery effectiveness of a_i, a_j, u_i, u_j, y_i, and y_j, and naturally, the position of the joint muscle can be recovered more accurately (see Fig. 5).

(2) Framework flexibility. In this work, we use a decoder based on the Wiener filter, an MPC controller and a spiking neuron network to formulate the closed-loop BMI frameworks. Note that, as closed-loop frameworks, they have obvious advantages, i.e., the decoder, auxiliary controller, and encoder can be flexibly replaced by other components with similar functions, and then various BMI systems can be designed according to the two frameworks.

(3) Algorithm complexity simplification. Because the PSO algorithm is adopted to solve the two optimization problems in the designed frameworks, the online computational complexity will be increased and the system running speed will be slowed down. This problem can be solved through the "offline optimization and online table lookup" strategy proposed in [35]. According to this strategy, we can offline formulate a lookup table first, in which the decision variables $\{a_1, a_2, w_1, w_2, w_3, w_4\}$ at k and $\mathbb{J}_p(k)$ have one-to-one corresponding relations. Then, when the system is online running, we can search the lookup table to find the minimum of $\mathbb{J}_p(k)$ and the corresponding $\{a_1, a_2, w_1, w_2, w_3, w_4\}$, then apply them to the frameworks. This strategy can significantly decrease the online computational burden.

6. Conclusions

In this paper, two closed-loop BMI frameworks are formulated based on a Wiener filter-based decoder, an MPC controller, a spiking neuron network-based encoder, and ICMS current technology. Specifically, the Wiener filter-based decoder is introduced to convert commands from the brain to the external device, the encoder and ICMS current are designed to feedback the state of the external device to the brain, and the auxiliary controller based on an MPC strategy is used to calculate the parameters of the ICMS current. The results of a simulation show that the designed BMI framework 2 can recover the motor function of the joint much better than framework 1.

CRediT authorship contribution statement

Hongguang Pan: Funding acquisition, Project administration, Supervision, Writing - review & editing, Conceptualization. **Wenyu Mi:** Methodology, Software, Data curation, Writing - original draft. **Xinyu Lei:** Writing - review & editing. **Jun Deng:** Writing - review & editing.

Acknowledgements

Conflicts of interest

The authors declare no conflicts of interest.

References

[1] J.E. O'Doherty, M.A. Lebedev, P.J. Ifft, K.Z. Zhuang, S. Shokur, H. Bleuler, M.A. Nicolelis, Active tactile exploration using a brain–machine–brain interface, Nature 479 (7372) (2011) 228–231.

[2] M.M. Shanechi, A.L. Orsborn, J.M. Carmena, Robust brain–machine interface design using optimal feedback control modeling and adaptive point process filtering, Plos Comput. Biol. 12 (4) (2016) e1004730.

[3] W. Zhang, F. Sun, H. Wu, C. Tan, Y. Ma, Asynchronous brain–computer interface shared control of robotic grasping, Tsinghua Sci. Technol. 24 (3) (2019) 360–370.

[4] L.W. Ko, Y.C. Lu, H. Bustince, Y.C. Chang, C.T. Lin, Multimodal fuzzy fusion for enhancing the motor-imagery-based brain computer interface, IEEE Comput. Intell. Mag. 14 (1) (2019) 96–106.

[5] M.V. Lukoyanov, S.Y. Gordleeva, A.S. Pimashkin, N.A. Grigor'ev, A.V. Savosenkov, A. Motailo, V.B. Kazantsev, A.Y. Kaplan, The efficiency of the brain–computer interfaces based on motor imagery with tactile and visual feedback, Hum. Physiol. 44 (3) (2018) 280–288.

[6] H. Pan, M. Wang, X. Wang, J.-S. Lin, EEG control variable algorithm and motion control strategy for toy rail car, Int. J. Embed. Syst. 20 (2) (2019) 220–228.

[7] H. Pan, W. Mi, F. Wen, W. Zhong, An adaptive decoder design based on the receding horizon optimization in BMI system, Cognit. Neurodyn. (2019), http://dx.doi.org/10.1007/s11571-019-09567-4.

[8] D.M. Lazurenko, V.N. Kiroy, I.E. Shepelev, L.N. Podladchikova, Motor imagery-based brain–computer interface: neural network approach, Opt. Memory Neural Netw. 28 (2) (2019) 109–117.

[9] J.P. Cunningham, P. Nuyujukian, V. Gilja, C.A. Chestek, S.I. Ryu, K.V. Shenoy, A closed-loop human simulator for investigating the role of feedback control in brain–machine interfaces, J. Neurophysiol. 105 (4) (2011) 1932–1949.

[10] M.C. Dadarlat, J.E. O'Doherty, P.N. Sabes, A learning-based approach to artificial sensory feedback, Nat. Neurosci. 18 (1) (2015) 138–144.

[11] R.L. Kæseler, K. Leerskov, L.A. Struijk, K. Dremstrup, M. Jochumsen, Designing a brain computer interface for control of an assistive robotic manipulator using steady state visually evoked potentials, 2019 IEEE 16th International Conference on Rehabilitation Robotics (ICORR) (2019) 1067–1072.

[12] Y. Xu, X. Wang, C. Peck, M.E. Goldberg, The time course of the tonic oculomotor proprioceptive signal in area 3a of somatosensory cortex, J. Neurophysiol. 106 (1) (2011) 71–77.

[13] S. Dangi, S. Gowda, R. Heliot, J.M. Carmena, Adaptive kalman filtering for closed-loop brain–machine interface systems, in: International IEEE/EMBS Conference on Neural Engineering, Cancun, Mexico, 2011 April.

[14] D. Sussillo, P. Nuyujukian, J.M. Fan, J.C. Kao, S.D. Stavisky, S. Ryu, K. Shenoy, A recurrent neural network for closed-loop intracortical brain–machine interface decoders, J. Neural Eng. 9 (2) (2012) 026027.

[15] S. Dangi, Closed-Loop Decoder Adaptation Algorithms for Brain–Machine Interface Systems, UC Berkeley, 2015, Ph.D. dissertation.

[16] A. Orsborn, Closed-Loop Design of Brain–Machine Interface Systems, UC Berkeley, 2013, Ph.D. Dissertation.

[17] N.S. Davidovics, G.Y. Fridman, B. Chiang, C.C. Della Santina, Effects of biphasic current pulse frequency, amplitude, duration, and interphase gap on eye movement responses to prosthetic electrical stimulation of the vestibular nerve, IEEE Trans. Neural Syst. Rehabil. Eng. 19 (1) (2011) 84–94.

[18] M.A. Nicolelis, M.A. Lebedev, Principles of neural ensemble physiology underlying the operation of brain–machine interfaces, Nat. Rev. Neurosci. 10 (7) (2009) 530–540.

[19] W. Gerstner, Spiking neuron models: single neurons, populations, plasticity, Kybernetes 32 (7/8) (2002) 277–280.

[20] R. Brette, M. Rudolph, T. Carnevale, M. Hines, D. Beeman, J.M. Bower, M. Diesmann, A. Morrison, P.H. Goodman, F.C. Harris Jr., et al., Simulation of networks of spiking neurons: a review of tools and strategies, J. Comput. Neurosci. 23 (3) (2007) 349–398.

[21] T.J. Foutz, C.C. Mcintyre, Evaluation of novel stimulus waveforms for deep brain stimulation, J. Neural Eng. 7 (6) (2010) 066008.

[22] J. Daly, J. Liu, M. Aghagolzadeh, K. Oweiss, Optimal space-time precoding of artificial sensory feedback through mutichannel microstimulation in bi-directional brain–machine interfaces, J. Neural Eng. 9 (9) (2012) 065004.

[23] J. Liu, H.K. Khalil, K.G. Oweiss, Neural feedback for instantaneous spatiotemporal modulation of afferent pathways in bi-directional brain–machine interfaces, IEEE Trans. Neural Syst. Rehabil. Eng. 19 (5) (2011) 521–533.

[24] S.F. Cogan, Neural stimulation and recording electrodes, Annu. Rev. Biomed. Eng. 10 (2008) 275–309.

[25] A.E. Hadjinicolaou, T.L. Ronald, J.G. David, G. Kumaravelu, F. Kate, A.N. David, N.S. Mohit, M. Hamish, R.I. Michael, P. Steven, Electrical stimulation of retinal ganglion cells with diamond and the development of an all diamond retinal prosthesis, Biomaterials 33 (24) (2012) 5812–5820.

[26] D.J. Weber, B.M. London, J.A. Hokanson, C.A. Ayers, R.A. Gaunt, R.R. Torres, B. Zaaimi, L.E. Miller, Limb-state information encoded by peripheral and central somatosensory neurons: implications for an afferent interface, IEEE Trans. Neural Syst. Rehabil. Eng. 19 (5) (2011) 501–513.

[27] D.Q. Mayne, J.B. Rawlings, C.V. Rao, P.O.M. Scokaert, Constrained model predictive control: stability and optimality, Automatica 36 (6) (2000) 789–814.

[28] H. Pan, W. Zhong, Z. Wang, Economic optimization and control based on multi priority rank RTO and double layered MPC, Asian J. Control 20 (6) (2018) 2271–2280.

[29] H. Pan, W. Zhong, Z. Wang, An on-line constraint softening strategy to guarantee the feasibility of dynamic controller in double-layered MPC, Chin. J. Chem. Eng. 25 (12) (2017) 1805–1811.

[30] H. Pan, M. Wang, Z. Wang, P. Wang, The performance comparison of two kinds of decoders in brain–machine interface, International Symposium on Computer, Consumer and Control (2016) 247–250.

[31] D. Bullock, P. Cisek, S. Grossberg, Cortical networks for control of voluntary arm movements under variable force conditions, Cereb. Cortex 8 (1) (1998) 48–62.

[32] W.H. Kwon, S. Han, Receding Horizon Control, Springer London, 2005.

[33] W. Zhong, S. Li, F. Qian, θ-PSO: a new strategy of particle swarm optimization, J. Zhejiang Univ. Sci. A 9 (6) (2008) 786–790.

[34] J.E. O'Doherty, M.A. Lebedev, P.J. Ifft, K.Z. Zhuang, S. Solaiman, B. Hannes, M.A.L. Nicolelis, Active tactile exploration using a brain–machine–brain interface, Nature 479 (7372) (2012) 228–231.

[35] H. Zheng, T. Zou, J. Hu, H. Yu, An offline optimization and online table look-up strategy of two-layer model predictive control, IEEE Access 6 (2018) 47,433–47,441.